Neutron multiplicity measurement and investigation of nuclear dissipation and shell effects in ^{30}Si + ^{182,184,186}W reactions

M. Shareef,[1,*] E. Prasad,[2,†] A. Jhingan,[3] N. Saneesh,[3,5] Santanu Pal,[4,‡] A. M. Vinodkumar,[5] K. S. Golda,[3] Mohit Kumar,[3] A. Shamlath,[2,§] P. V. Laveen,[2,‖] A. C. Visakh,[2] M. M. Hosamani,[6] S. K. Duggi,[7] P. Sandya Devi,[7] G. N. Jyothi,[7] A. Tejaswi,[7] A. Chatterjee,[3] and P. Sugathan[3]

[1]*Saha Institute of Nuclear Physics, 1/AF, Bidhan Nagar, Kolkata 700064, India*
[2]*Department of Physics, School of Physical Sciences, Central University of Kerala, Kasaragod 671316, India*
[3]*Inter-University Accelerator Centre, Aruna Asaf Ali Marg, New Delhi 110067, India*
[4]*CS-6/1, Golf Green, Kolkata 700095, India*
[5]*Department of Physics, University of Calicut, Calicut 673635, India*
[6]*Department of Physics, Karnatak University, Dharwad 580003, India*
[7]*Department of Nuclear Physics, Andhra University, Visakhapatnam 530003, India*

(Received 15 December 2022; revised 22 April 2023; accepted 10 May 2023; published 30 May 2023)

Background: Enhanced prescission neutron multiplicity ($\nu_{\rm pre}$) over statistical model calculations assuming Bohr-Wheeler fission width is explained using Kramers' fission width incorporating dissipative effects. The dissipation strength obtained from such studies reported significant effect of the neutron shell closure of $N = 126$ of the fissioning system as well as nuclear temperature. The dependence of dissipation strength on shell effect and temperature is also attributed to the choice of input parameters in the statistical model calculations.
Purpose: We investigate the role of N/Z, shell effect, collective enhancement of level density (CELD), and excitation energy on $\nu_{\rm pre}$ in reactions forming isotopes of the Ra nucleus.
Methods: The neutron multiplicity excitation function is measured for the ^{30}Si + ^{182,184,186}W reactions populating ^{212,214,216}Ra nuclei using the National Array of Neutron Detectors (NAND) at the Inter-University Accelerator Centre, New Delhi. Among these compound nuclei, ^{214}Ra has a major neutron shell closure of $N = 126$. Measured $\nu_{\rm pre}$ are analyzed within the framework of a statistical model incorporating dynamical hindrance in nuclear fission due to dissipation, shell corrections in the fission barrier and level density, and CELD.
Results: Experimental $\nu_{\rm pre}$ show a marginal isotopic dependence at all excitation energies. $\nu_{\rm pre}$ values do not show any noticeable effect of neutron magic number $N = 126$. Dissipation strength of $\beta = 8$ zs^{-1} (5.27 MeV/$\hbar$) reasonably reproduces the experimental $\nu_{\rm pre}$ excitation functions for all three nuclei in the measured energy range. Appreciable variations in presaddle neutron emissions are observed when shell effect or CELD is excluded in the calculations. Even though both the shell and CELD are found to impact primarily in the presaddle sector, they alter the excitation energy and multiplicity in the saddle-to-scission sector as well in a complementary manner.
Conclusions: A temperature independent dissipation coefficient is observed to reproduce the experimental results in this study throughout the excitation energy range measured. Shell corrections in fission barrier and level density parameters and CELD in fission and particle evaporation widths also influence the neutron multiplicities. The observed effect of CELD in the presaddle phase is attributed to the large enhancement of level density at the saddle due to its large deformation and consequent enhancement of fission width.

DOI: 10.1103/PhysRevC.107.054619

I. INTRODUCTION

Even eight decades after its discovery, nuclear fission continues to be a challenging field of research in physics. Fission displays a large-scale rearrangement of strongly interacting matter distribution involving a complex interplay between dynamical and structural effects. The fascinating story of nuclear fission in the early years can be found in Ref. [1] and a detailed account of its present status in Ref. [2].

One of the early surprises in heavy-ion induced fission of highly excited compound nuclei was the observation that the prescission multiplicities of neutrons, light charged particles, and γ rays are higher than those predicted by the

*shareef.m.cuk@gmail.com; Formerly at Department of Physics, School of Physical Sciences, Central University of Kerala, Kasaragod 671316, India.
†Corresponding author: prasadenair@cukerala.ac.in
‡Formerly with Physics Group, VECC, Kolkata 700064, India.
§Present address: Institute for Integrated Programmes and Research in Basic Sciences (IIRBS), Mahatma Gandhi University, Kottayam 686560, India.
‖Present address: Department of Physics, Kannur University Swami Anandatheertha Campus, Payyanur 670327, Kerala, India.

transition-state theory of fission, which consequently suggests a fission hindrance or a dissipative dynamics of fission [3–6]. A dissipative drag in nuclear dynamics arises from the coupling of the collective motion with the intrinsic degrees of freedom of the nuclei [7]. Stochastic dynamical models for fission based on Langevin equations have been developed in order to calculate various experimental observables including prescission multiplicities, evaporation residue (ER) cross sections, and fission fragment mass-energy, charge, and angular distributions [8–10]. Alternatively, one can use the fission width given by Kramers [11], which includes the effect of dissipation, in a statistical model of nuclear decay. One of the early uses of Kramers's width in a statistical model was by Newton *et al.* [12], and since then it has been used in numerous works. The dissipation strength is an essential input to both the dynamical and statistical model calculations.

A statistical model analysis of the ER cross sections of a number of compound nuclei (CN) was made by Back *et al.* [13] using the dissipation coefficient as an adjustable parameter to fit the experimental data. An excitation energy dependence of the dissipation coefficient was observed. Dioszegi *et al.* [14] made a detailed statistical model analysis of the prescission neutron and γ-ray multiplicities along with the evaporation residue (ER) cross sections off the compound nucleus ^{224}Th, and found that a CN temperature dependence of the dissipation coefficient is necessary to fit the data. An excitation energy dependent dissipation strength was used to reproduce the multiplicities of prescission neutrons from a number of hot Fr isotopes [15]. A similar observation was also made in the statistical model analyses of prescission neutron multiplicities from a chain of Rn isotopes populated in fusion-fission reactions [16]. A Langevin dynamical calculation for prescission neutron multiplicity from the compound nucleus ^{208}Rn was made by Neeraj *et al.* [17], and an excitation energy dependent dissipation was found to be necessary to fit the data. In a different approach, an energy independent fixed value for dissipation was used in statistical model calculations for prescission neutron multiplicity and fission/ER cross sections where two adjustable parameters, which effectively control the level density and fission barrier, were used to fit the data [18,19]. No excitation energy dependence of the dissipation strength was observed in statistical model calculations for prescission neutron numbers from the compound nucleus ^{227}Np [20]. The collective enhancement of level density (CELD) and the effect of tilting away of CN spin orientation were included in this statistical model calculation. Evidently the dissipation strength, when used as an adjustable parameter, depends on the choice of other input parameters in a calculation.

Theoretical guidance regarding the strength of the dissipative force in nuclear dynamics is mostly provided by the so-called one-body model of nuclear dissipation [7]. This classical macroscopic one-body dissipation strength has no dependence on the excitation energy of the nucleus. The microscopic quantum mechanical version of one-body dissipation, however, is very small at low excitations and increases towards the classical one-body dissipation with increasing temperature [21]. Three-dimensional (3D Langevin dynamical calculations of fission fragment total kinetic energy (TKE) systematics show better agreement with the experimental data with microscopic rather than macroscopic dissipation [22]. However, similar calculations in 4D reproduce the TKE systematics reasonably well with macroscopic dissipation also [23]. The nature and magnitude of nuclear dissipation thus remains an open question.

Shell effects are known to play a major role in low energy fission [24]. The asymmetric mass divisions in low energy fission of actinide [24,25] and preactinide [26–28] nuclei are attributed to shell effects. However, shell effects are not directly revealed in experimental observables in fission of highly excited nuclei. Theoretical analysis is necessary to decipher shell effects in experimental data. In the theoretical modeling of the decay of a hot compound nucleus, shell effects are generally included in the nuclear level density and the fission barrier. Since nuclear dissipation accounts for the coupling between the intrinsic and collective motion, one might expect that shell structure in single-particle states can leave some signature in the dissipation strength. Shell effects are thus sought in the dissipation strength which best fits the experimental data. Statistical model analyses of evaporation residue (ER) cross sections in an earlier work showed a strong effect of neutron shell closure on the dissipation strength [13]. It was further observed that the dissipation strength shows a strong isotopic dependence when no shell effects were considered in a statistical model calculation of prescission neutron multiplicities from a chain of Fr isotopes formed in fusion-fission reactions [15]. When shell effects were included in the calculations, the extracted dissipation strengths of the different isotopes became very close to each other, though slightly lower values for the neutron closed shell CN ^{213}Fr were noticed in the above work. Seemingly, the extracted dissipation strength and its shell dependence depend on the choice of the other input parameters in the statistical model calculations. A marginal dip in the dissipation strength for the neutron closed shell compound nucleus ^{212}Rn was also observed in a statistical model analysis of prescission neutrons from a series of Rn isotopes [16].

Prescission neutrons are emitted during the entire period of evolution of the CN from the ground state to the scission configuration. Thus, the prescission neutron multiplicity is more suitable as a probe for nuclear dissipation operating in nuclear dynamics from saddle to scission, compared to fission/ER cross sections which are sensitive to the nuclear dynamics only up to the saddle configuration. As stated earlier, shell structure in the single-particle spectra might influence the dissipation strength, hence it is of considerable interest to explore the effect of increasing N/Z of compound nuclei for a given element on the strength of nuclear dissipation. Further, the magnitude and excitation energy dependence of dissipation is crucial to understand the mechanism of dissipation. In order to address the above queries, it is necessary to measure the excitation functions of prescission neutrons from an isotopic chain and extract the dissipation strength from fitting the data.

In the present work, we shall report the experimental measurement of neutron multiplicity from the reactions $^{30}\mathrm{Si} + ^{182,184,186}\mathrm{W}$ populating the compound nuclei ^{212,214,216}Ra in the excitation energy range of 45–95 MeV. Radium comes immediately after radon and francium in the

periodic table, which have been extensively studied in earlier works [15,16]. ^{214}Ra is a neutron closed shell ($N = 126$) nucleus and provides an opportunity to study shell effects by comparing the data with the other two non-closed-shell nuclei. We shall perform statistical model analysis of the pre-scission multiplicity from the three reactions and look for excitation energy dependence and shell effects in the results. The statistical model employed in the present work has additional features, namely the collective enhancement of level density and the effect due to tilting of CN spin orientation, which were not included in the statistical model analyses reported earlier [15,16]. We therefore expect that the present analysis would provide a better estimate of the dissipation strength.

The paper is organized as follows. The experimental details are presented in Sec. II. The data analysis and the experimental results are given in Sec. III. Section IV contains the details of the statistical model used in the present work. The statistical model results are presented and discussed in Sec. V. The work is summarized in the last section.

II. EXPERIMENTAL DETAILS

The experiments were performed using pulsed beams of ^{30}Si from the 15 UD Pelletron+Superconducting Linear Accelerator facility of the Inter-University Accelerator Centre (IUAC), New Delhi. Beams with a pulse separation of 250 ns were used in the experiment to bombard isotopically enriched targets of ^{182,184,186}W having thicknesses of 405, 450 and 331 μg/cm^2, respectively. All three targets had a carbon backing of thickness 25 μg/cm^2. The measurements were performed in the excitation energy range of 45 to 95 MeV.

The schematic of the experimental setup used in the present study is reported elsewhere [20]. The targets were mounted normal to the beam direction at the center of a 100 cm diameter spherical scattering chamber. Two silicon surface barrier detectors were placed at ±12.5° with respect to the beam direction, inside the scattering chamber, to detect the elastically scattered beam particles. The Rutherford events registered by these detectors were used for beam monitoring as well as positioning the beam at the center of the target. The complementary fragments from fission or fissionlike events were detected using a pair of identical position-sensitive multiwire proportional counters (MWPCs) with 11×16 cm^2 active area. These MWPCs were mounted at ±69° (laboratory angle) with respect to beam direction at either side such that the complementary fragments are detected. These detectors were operated with isobutane gas at 3.5 mbar gas pressure.

A time-of-flight (ToF) spectrum was generated using the timing signals of the two MWPCs. Fission fragments (FFs) are well separated from the elastics or recoils reaching the detectors. Figure 1 shows two-dimensional correlated ToF spectra from the two MWPCs for the ^{30}Si + ^{184}W reaction at $E_{\rm lab} = 158.8$ MeV.

Neutrons emitted during various stages of the fusion-fission reaction and postfission fragments were detected in coincidence with the complementary fission fragments using 50 organic liquid scintillator detectors (BC 501A) of the National Array of Neutron Detectors (NAND) facility [29]. These detectors were mounted at different polar (θ) and azimuthal (ϕ) angles with respect to the beam direction as given in Ref. [20].

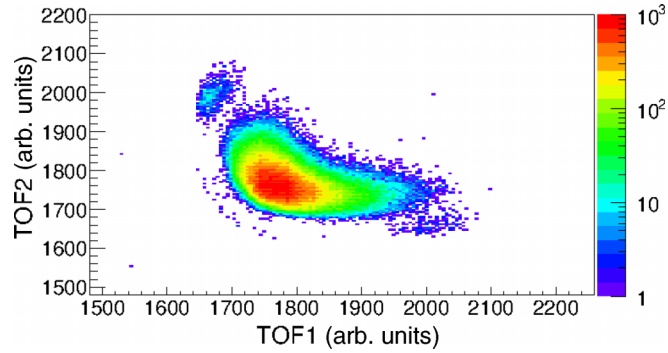

FIG. 1. Scatter plot of ToF spectra of the complementary fragments detected in the two MWPC detectors for the ^{30}Si + ^{184}W reaction at $E_{\rm lab} = 158.8$ MeV.

The measurement of intrinsic efficiency of these neutron detectors is discussed elsewhere [20]. The pulse shape discrimination (PSD) method based on the zero-crossover technique together with the ToF was used for a clear identification of the neutrons from the γ rays [30]. A typical spectrum of ToF versus PSD from one of the neutron detectors for the ^{30}Si + ^{184}W reaction at $E_{\rm lab} = 158.8$ MeV is shown in Fig. 2. The logical OR of the timing signal of two fission fragments AND-ed with the radio frequency signal formed the trigger for the data acquisition system. This logical signal was used as the master start of the time-to-digital converter as well as the master gate for all the analog-to-digital converter used.

III. DATA ANALYSIS AND RESULTS

The prescission and postscission neutron multiplicities and temperature (CN and FFs) were obtained by the spectral deconvolution of the measured double differential neutron multiplicity spectra. Neutrons are assumed to be emitted from the three moving sources—the CN and the complementary FFs—and are assumed to be in thermal equilibrium. The neutron emission from these three sources is assumed to be isotropic in their rest frames. Further, symmetric fragment mass split [31] is assumed. Measured neutron spectra consist

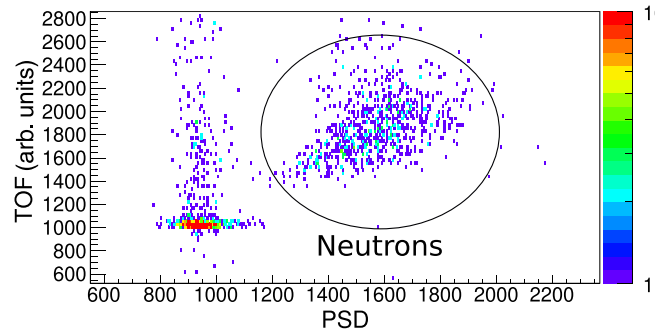

FIG. 2. Pulse shape discrimination (PSD) versus time of flight (ToF) spectra from one of the neutron detectors for the ^{30}Si + ^{184}W reaction at $E_{\rm lab} = 158.8$ MeV.

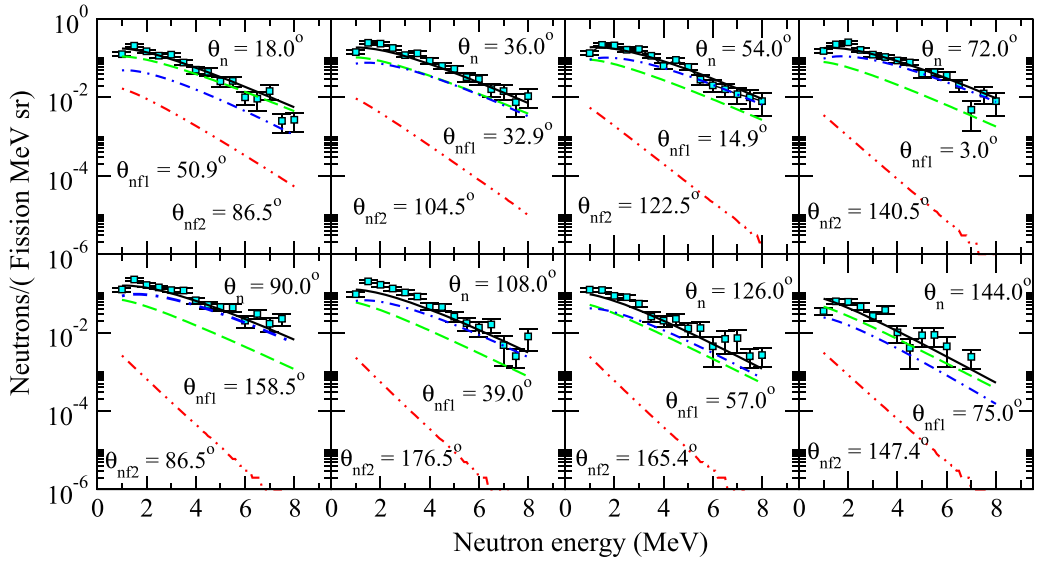

FIG. 3. Experimental double differential neutron multiplicity spectra (solid circles) for the $^{30}\mathrm{Si} + ^{182}\mathrm{W}$ reaction at an excitation energy of 76.0 MeV for eight neutron detectors in the reaction plane. The multiple-moving-source fits for the prescission (dashed lines) and postscission contributions from one fragment (dott-dashed lines) and that from the other (dot-dot-dashed lines) are also shown. The total contribution from all the three sources is indicated by the solid line.

of pre-scission neutrons emitted from the CN before scission and the postscission neutrons emitted from the fast moving fission fragments [33] after scission.

Prescission and postscission neutron multiplicities and temperatures were extracted from the experimental neutron energy spectra, using the multiple source fitting of the Watt expression [32,33], given by

$$\frac{d^2M}{dE_n d\Omega_n} = \sum_{i=1}^{3} \frac{\nu_i \sqrt{E_n}}{2(\pi T_i)^{3/2}} \times \exp\left[-\frac{E_n - 2\sqrt{E_n E_i/A_i}\cos\theta_i + E_i/A_i}{T_i}\right], \quad (1)$$

where E_n is the neutron energy in the laboratory frame, and ν_i, A_i, E_i, and T_i are the neutron multiplicity, mass, kinetic energy, and temperature, respectively of each neutron emitter. θ_i is the angle between the direction of the emitted neutron and its source.

The kinetic energies of the fission fragments, E_{FF}, were obtained from the Viola systematics [31]. Folding angles of the binary fission fragments were calculated assuming full momentum transfer. Angles between the emitted neutrons and their sources were determined from the scalar product of the unit vectors along the neutron direction and the source (CN or fission fragments).

For the spectrum deconvolution, we limited the neutron energy between 1 and 8 MeV in this work. This would exclude the possible contributions of neutrons from undesired processes such as preequilibrium emission [34] in the analysed spectra. The pre- and postscission components of neutron multiplicities and temperatures were obtained from the simultaneous fitting of neutron energy spectra, after the efficiency correction.

The fitting was performed considering ν_{pre}, ν_{post}, T_{pre}, and T_{post} as free parameters in the beginning. Fitting is also performed by fixing the temperature of the CN as [35]

$$T_{\mathrm{pre}} = \frac{11}{12}\sqrt{\frac{E^*}{a}}, \quad (2)$$

where E^* is the CN excitation energy and a is the level density parameter assumed to be $a = \frac{A_{CN}}{9}$ MeV^{-1} [36]. Both of these approaches yielded the same results, consistent with previous observations [20].

The best fits of the double differential neutron multiplicity spectra and their components for the $^{30}\mathrm{Si} + ^{182}\mathrm{W}$ reaction are shown in Fig. 3, as an example. The error bars in the figure represent the statistical uncertainties. Although the spectra from 50 detectors were simultaneously fitted, the figure shows only a sample of eight detectors. The total average neutron multiplicity ν_{tot} is obtained from the fitted values of ν_{pre} and T_{post} as $\nu_{\mathrm{tot}} = \nu_{\mathrm{pre}} + 2\nu_{\mathrm{post}}$. The best fit values of ν_{tot}, ν_{pre}, ν_{post}, T_{pre}, and T_{post} obtained for the $^{30}\mathrm{Si} + ^{182,184,186}\mathrm{W}$ reactions are summarized in Table I.

Besides fusion-fission, competing processes such as quasifission could also contribute to the measured neutron multiplicities. A significant effect of quasifission in prescission neutron multiplicity was reported for the $^{58}\mathrm{Ni} + ^{208}\mathrm{Pb}$ [37] and $^{48}\mathrm{Ti} + ^{208}\mathrm{Pb}$ [38] reactions earlier. Being mass symmetric, fast quasifission is expected in these systems, where the dinuclear system reseparates soon after capture. Onset of quasifission was reported for the $^{30}\mathrm{Si} + ^{186}\mathrm{W}$ reaction [39], which predominantly populates the mass-symmetric region and hence overlaps completely with fusion-fission events. The presence of such nonequilibrium events led to increased mass-width in this reaction compared to other more asymmetric entrance channels populating the same CN [39]. Based on

TABLE I. Reactions considered for the neutron multiplicity measurements in this work populating CNs with different N/Z values. Measured E_{lab} and the values of ν_{pre}, ν_{post}, ν_{total}, T_{pre}, and T_{post} obtained from the measurements are tabulated.

Reactions	CN	N/Z	E_{lab} (MeV)	E^* (MeV)	ν_{pre} (±err)	ν_{post} (±err)	ν_{total} (±err)	T_{pre} (MeV) (±err)	T_{post} (MeV) (±err)
$^{30}Si + ^{182}W$	^{212}Ra	1.409	138.8	46.7	1.34	0.87	3.08	1.23	0.89
					(0.12)	(0.04)	(0.13)	(0.06)	(0.04)
			151.8	57.9	1.99	0.97	3.93	1.25	0.90
					(0.10)	(0.04)	(0.11)	(0.05)	(0.02)
			158.8	63.9	2.14	1.04	4.22	1.29	0.93
					(0.11)	(0.04)	(0.12)	(0.04)	(0.02)
			165.9	69.9	2.41	1.02	4.45	1.36	0.99
					(0.12)	(0.05)	(0.13)	(0.05)	(0.03)
			172.9	76.0	2.75	1.09	4.93	1.37	1.00
					(0.13)	(0.05)	(0.14)	(0.04)	(0.05)
			178.9	81.1	2.95	1.03	5.01	1.47	1.00
					(0.15)	(0.06)	(0.17)	(0.05)	(0.04)
			185.9	87.2	3.19	1.13	5.45	1.48	1.03
					(0.17)	(0.06)	(0.19)	(0.06)	(0.04)
			191.9	92.3	3.25	1.19	5.63	1.50	1.10
					(0.19)	(0.08)	(0.22)	(0.06)	(0.05)
$^{30}Si + ^{184}W$	^{214}Ra	1.431	138.7	49.0	1.61	0.83	3.27	1.26	0.88
					(0.12)	(0.05)	(0.13)	(0.08)	(0.04)
			144.7	54.2	2.04	0.82	3.68	1.28	0.90
					(0.13)	(0.05)	(0.14)	(0.06)	(0.04)
			151.7	60.3	2.22	0.93	4.08	1.30	0.92
					(0.12)	(0.04)	(0.13)	(0.05)	(0.03)
			158.8	66.3	2.35	1.01	4.37	1.31	0.94
					(0.12)	(0.04)	(0.13)	(0.04)	(0.03)
			165.8	72.3	2.63	1.10	4.83	1.33	0.94
					(0.13)	(0.05)	(0.14)	(0.05)	(0.03)
			178.8	83.5	3.16	1.15	5.46	1.41	1.00
					(0.16)	(0.06)	(0.18)	(0.05)	(0.04)
			185.9	89.6	3.67	1.08	5.83	1.50	1.02
					(0.17)	(0.07)	(0.19)	(0.05)	(0.05)
			191.9	94.8	3.84	1.16	6.16	1.53	1.05
					(0.18)	(0.07)	(0.20)	(0.05)	(0.05)
$^{30}Si + ^{186}W$	^{216}Ra	1.454	139.0	49.5	1.96	0.82	3.60	1.23	0.77
					(0.11)	(0.04)	(0.12)	(0.05)	(0.03)
			145.0	54.6	2.17	0.88	3.93	1.29	0.84
					(0.12)	(0.04)	(0.13)	(0.06)	(0.03)
			152.0	60.7	2.31	0.96	4.23	1.30	0.96
					(0.13)	(0.05)	(0.14)	(0.05)	(0.03)
			159.1	66.7	2.66	0.99	4.64	1.32	0.90
					(0.14)	(0.04)	(0.15)	(0.05)	(0.03)
			166.1	72.8	2.85	1.00	4.85	1.39	0.91
					(0.15)	(0.05)	(0.16)	(0.05)	(0.03)
			173.1	78.8	3.28	1.05	5.38	1.42	0.97
					(0.15)	(0.06)	(0.17)	(0.04)	(0.04)
			179.1	84.0	3.36	1.16	5.68	1.41	1.01
					(0.17)	(0.06)	(0.19)	(0.05)	(0.04)
			186.1	90.0	4.17	1.01	6.19	1.51	1.00
					(0.19)	(0.07)	(0.21)	(0.05)	(0.05)

the systematic study of quasifission timescales [40,41] and the experimental signatures reported in Ref. [39], the presence of slow quasifission is assumed in $^{30}Si + ^{182,184,186}W$ reactions, where the sticking time of the composite system is much longer than fast quasifission.

In order to check the possible contribution of quasifission in the measured neutron multiplicity, least-squares multi-source fits of neutron energy spectra were performed within a specific fragment mass window as in Refs. [42,43]. In the analysis, mass gates were applied between the mass ratio

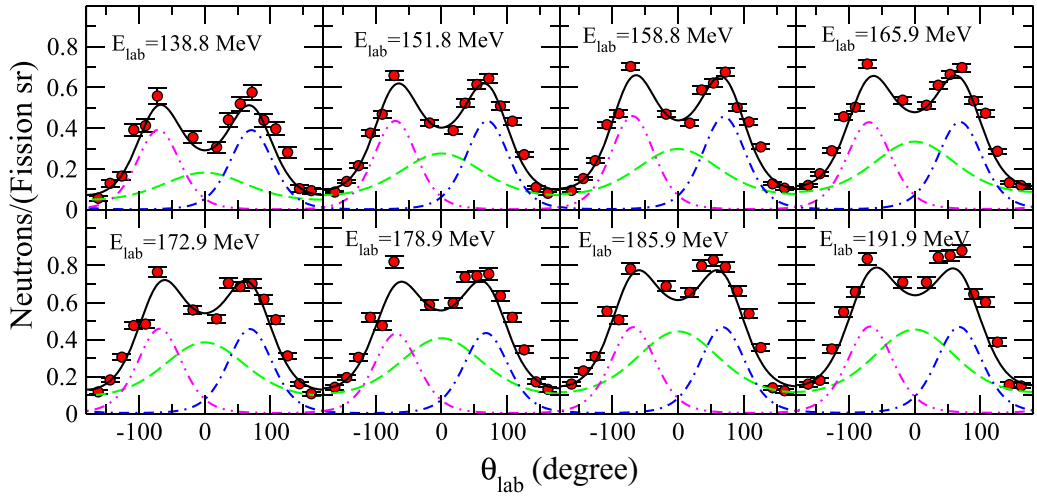

FIG. 4. Experimental neutron angular distribution (solid circles) along with that generated using the moving-source model (black solid line) for the $^{30}\mathrm{Si} + ^{182}\mathrm{W}$ reaction at different beam energies. Angular distributions of neutrons emitted from three sources mentioned in the text are also shown. The dashed line represents contribution from the CN; dot-dot-dashed and dot-dashed lines indicate the contributions from the complementary fission fragments, respectively.

values (ratio of fragment mass to the total mass of the fissioning nucleus) 0.4 and 0.6 while obtaining the ν_{pre} values. These gates were selected to distinguish symmetric fission and quasifission events. The neutron multiplicity values obtained with and without above mass gates, however, were found to be similar, within the experimental uncertainties. We could not differentiate the contribution from quasifission events to the total neutron multiplicity, unlike that reported in Refs. [37,38] in these reactions. This could be due to the comparable sticking times associated with the slow quasifission and fusion-fission process [41].

The angular distribution of neutrons along with those generated using the moving-source model, which considers three neutron emitting sources—the CN and two complementary FFs—are shown in Fig. 4 for the $^{30}\mathrm{Si} + ^{182}\mathrm{W}$ reaction. The contributions from different sources are also shown in the same figure. The emission spectra of neutrons from these respective sources were modeled according to the Eq. (1). The calculations were performed for the angular range of 0^0 to 180° with respect to the beam direction, on either side, for zero azimuthal angles (corresponding to the in-plane detectors). Neutron contributions from the CN and the complementary FFs are quite clear in Fig. 4, and the angular distribution from each neutron emitting source has a Gaussian distribution. The kinematic focusing effect of the fast moving sources may be noticed in the angular distributions: the neutrons emitted from the CN peak around the beam direction, while neutrons from the fragments peak around the mean detector angles.

Experimental prescission and total neutron multiplicities for the $^{30}\mathrm{Si} + ^{182,184,186}\mathrm{W}$ reactions are shown in Fig. 5. The error bars shown on the measured ν_{pre} and ν_{tot} are due the statistical uncertainties. The ν_{pre} values increase with increasing E^* of the CN. No noticeable effect of the neutron shell closure at $N = 126$ was observed in this study, in the E^* range measured. However, a marginal isotopic dependence is observed in the measured ν_{pre} values: larger ν_{pre} value is observed for systems with larger value of N/Z (of the CN) at all E^*.

IV. THE STATISTICAL MODEL

Experimental ν_{pre} excitation functions are analysed using the statistical model code VECSTAT [44]. This code simulates the decay of a compound nucleus by the Monte Carlo technique. The various decay widths of the CN are used for the simulation. The evaporation of neutrons, light charged particles, γ rays, and fission are considered as the decay modes of the CN. The particle and GDR γ emission widths are

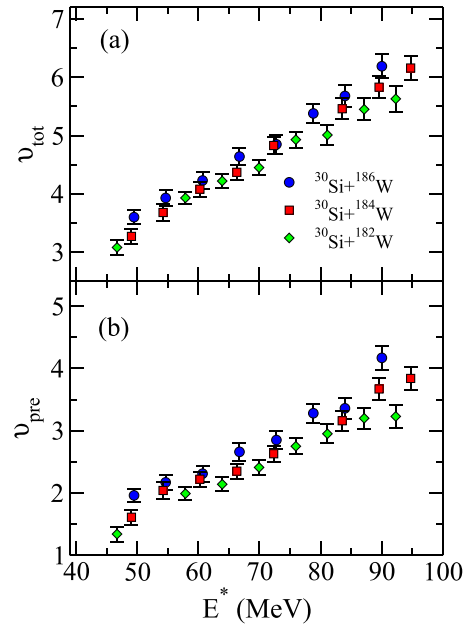

FIG. 5. Experimental ν_{tot} and ν_{pre} for $^{30}\mathrm{Si} + ^{182,184,186}\mathrm{W}$ reactions at different E^* are shown in panels (a) and (b), respectively.

obtained from the Weisskopf formula [45] as given in Ref. [9]. It may be mentioned here that the neutron and light charged particle scattering cross sections appearing in the respective width expressions are taken from the parametrization due to Blann [46]. The fission width is taken from the work of Kramers [11], in which the effect of dissipative fission dynamics is included. The contribution of $K \neq 0$ values to the fission width is also included, where K is the component of CN angular momentum along the nuclear symmetry axis [47]. The fission width of a CN at excitation energy E^* and carrying angular momentum l is then given as

$$\Gamma_f(E^*, l) = K_f \Gamma_{BW}(E^*, l) \left\{ \sqrt{1 + \left(\frac{\beta}{2\omega_s}\right)^2} - \frac{\beta}{2\omega_s} \right\}, \quad (3)$$

where β is the reduced dissipation coefficient (ratio of dissipation coefficient to collective inertia). ω_s is the frequency of the harmonic oscillator potential which approximates the nuclear potential in the saddle region and depends on the CN angular momentum (l) [48]. The Bohr-Wheeler fission width is given as [49]

$$\Gamma_{BW}(E^*, l) = \frac{1}{2\pi \rho_g(E^*, l)} \int_0^{E^* - B_f(l)} \rho_s(E^* - B_f(l) - \epsilon, l) d\epsilon, \quad (4)$$

where ρ_g and ρ_s denote the level densities at the ground state and saddle configurations, respectively, and $B_f(l)$ is the angular-momentum dependent fission barrier. Here, it is assumed that the spin of the CN remains perpendicular to the symmetry axis throughout the course of the reaction ($K = 0$).

The K-equilibration factor K_f is taken from Ref. [47]. The inclusion of K degree of freedom results in a reduction of the fission width compared to that obtained with $K = 0$. This is because, the fission barrier for the $K \neq 0$ states is higher than that with $K = 0$ state. The initial angular momentum distribution of the compound nuclei formed after capture in the entrance channel is calculated from the coupled channel code CCFULL [50]. The Akyuz-Winther parametrization [51] of optical model potential is used in CCFULL and is found to well reproduce the experimental fusion excitation function of the $^{30}\mathrm{Si} + ^{186}\mathrm{W}$ system [52]. The same potential parameters are also used for the $^{30}\mathrm{Si} + ^{182,184}\mathrm{W}$ systems.

The macroscopic part of the fission barrier used to calculate Γ_{BW} is obtained from the finite range liquid drop model (FRLDM) of the nuclear potential [53]. The shell correction is added to the FRLDM barrier [$B_f^{\mathrm{LDM}}(l)$] to give the full barrier as [54]

$$B_f(l) = B_f^{\mathrm{LDM}}(l) - (\delta_g - \delta_s). \quad (5)$$

Here δ_g and δ_s are the shell corrections at equilibrium and saddle deformations, respectively. The deformation dependent shell corrections δ_g and δ_s are obtained from Ref. [55] which suggests negligible shell correction at large deformations and full shell correction at zero deformation of the CN shape.

Following the work of Ignatyuk *et al.* [56], an energy dependent shell correction to the level density parameter is applied in the present work. According to this work, the shell effect is strongest at low excitation energies and washes out at high excitations. The energy dependent level density parameter is given as

$$a(E_{th}) = \tilde{a}\left(1 + \frac{f(E_{th})}{E_{th}}\delta_g\right), \quad (6)$$

with

$$f(E_{th}) = 1 - \exp(-E_{th}/E_D), \quad (7)$$

where E_{th} is the thermal part of the excitation energy and $\tilde{a}$ is the asymptotic value of level density parameter. E_D is the damping factor determining the rate of melting away of the shell effect with increasing excitation, and its value is taken to be 18.5 MeV [57]. We use the deformation dependent level density parameter $\tilde{a}$ given in Ref. [57].

It was shown earlier that the nuclear collective (rotational and vibrational) motion causes an enhancement of nuclear level density with respect to the intrinsic level density $\rho_{\mathrm{intr}}(E_{th})$ of a nucleus [58]. The inclusion of collective enhancement of level density (CELD) in statistical model calculations was found to be necessary for consistent reproduction of experimental observables [59]. We therefore also used CELD in the present calculations.

With inclusion of CELD, the total level density $\rho(E_{th})$ is given as

$$\rho(E_{th}) = K_{\mathrm{coll}}(E_{th}) \rho_{\mathrm{intr}}(E_{th}), \quad (8)$$

where $K_{\mathrm{coll}}(E_{th})$ is the collective enhancement factor [60] due to collective vibrations (K_{vib}) and rotations (K_{rot}) of the nucleus. A transition from vibrational to rotational enhancement with increasing quadrupole deformation ($|\beta_2|$) is made using a smooth transition function $\varphi(|\beta_2|)$ as follows [61]:

$$K_{\mathrm{coll}}(|\beta_2|) = [K_{\mathrm{rot}} \varphi(|\beta_2|) + K_{\mathrm{vib}}(1 - \varphi(|\beta_2|))] f(E_{th}), \quad (9)$$

where

$$\varphi(|\beta_2|) = \left[1 + \exp\left(\frac{\beta_2^o - |\beta_2|}{\Delta\beta_2}\right)\right]^{-1}, \quad (10)$$

where the values of β_2^o and $\Delta\beta_2$ are set to be 0.15 and 0.04, respectively [62]. A damping of collective effects [63] with increasing E^* is implemented using a Fermi function $f(E^*)$,

$$f(E_{th}) = \left[1 + \exp\left(\frac{E_{th} - E_{cr}}{\Delta E}\right)\right]^{-1} \quad (11)$$

where $E_{cr} = 40$ MeV and $\Delta E = 10$ MeV [63]. The rotational and vibrational enhancement factors considered are [60]

$$K_{\mathrm{rot}} = \frac{\tau_\perp T}{\hbar^2}, \quad (12)$$

$$K_{\mathrm{vib}} = e^{0.055 \times A^{2/3} \times T^{4/3}}, \quad (13)$$

where A is the mass number, T is the nuclear temperature, and $\tau_\perp$ is the rigid body moment of inertia perpendicular to the nuclear symmetry axis. The level density with CELD along with the shell corrected level density parameter is used to calculate the widths of all decay channels including fission.

In a stochastic dynamical model [64] of fission, a certain time interval elapses before fission rate reaches its stationary

value. We used the following parametrized form of time dependent fission width [$\Gamma_f(t)$] [65] in this work:

$$\Gamma_f(E^*, l, t) = \Gamma(E^*, l)\{1 - e^{-\frac{2.3t}{\tau_f}}\}, \tag{14}$$

where τ_f is the transient time period.

According to the transition-state model of fission [11,49], fission occurs when the CN crosses the saddle-point deformation. Therefore when an event is signaled as a fission event in the statistical model calculation, the number of neutrons emitted till that instant corresponds to the presaddle emissions. However, the evaporation process continues in the postsaddle sector till the scission configuration is reached. The number of neutrons emitted in the presaddle sector and those during the saddle-to-scission transition together make the multiplicity of the prescission neutrons. Thus, for a fission event, the evaporation process is followed for a time interval τ_{ss} during which the CN evolves from the saddle to the scission configuration. The following expression for τ_{ss} [66] is used in the present work:

$$\tau_{ss} = \tau_{ss}^0 \left\{ \sqrt{1 + \left(\frac{\beta}{2\omega_s}\right)^2} + \frac{\beta}{2\omega_s} \right\}, \tag{15}$$

Details of the above features are incorporated in the code VECSTAT and can be found in Refs. [44,59]. Calculations of the excitation functions of ν_{pre} using this code were performed and are presented in the next section.

V. STATISTICAL MODEL CALCULATIONS AND RESULTS

Statistical model (SM) calculations are made for prescission neutron multiplicities from the compound nuclei ^{212,214,216}Ra populated through the $^{30}\text{Si} + ^{182,184,186}\text{W}$ reactions, and the results are compared with the experimental values in Fig. 6. Excitation functions of ν_{pre} obtained with $\beta = 0, 4, 8$ zs^{-1} (0, 2.63, 5.27 MeV/$\hbar$) are shown. The statistical model predictions with Bohr-Wheeler fission width ($\beta = 0$) considerably underestimates ν_{pre} for all the three CN as shown in panels (a), (b), and (c) of Fig. 6. With increasing β, the calculated ν_{pre} excitation functions move closer to the experimental ones. It is observed that statistical model results with $\beta = 8$ zs^{-1} (5.27 MeV/$\hbar$) give reasonable agreement with the experimental data. The calculated multiplicities of neutrons emitted during the saddle-to-scission transition ($\nu_{\text{sad-sci}}$) and in the presaddle stage ($\nu_{\text{pre-sad}}$) are shown in panels (d), (e), (f) and panels (g), (h), (i) respectively. $\nu_{\text{sad-sci}}$ increases faster with excitation energy compared to $\nu_{\text{pre-sad}}$. Both $\nu_{\text{sad-sci}}$ and $\nu_{\text{pre-sad}}$ increase with the dissipation strength.

We thus find here an excitation energy independent value of 8 zs^{-1} (5.27 MeV/$\hbar$) for β for all three compound nuclei in the isotopic chain of Ra. However, earlier statistical model analyses of prescission neutron multiplicities from isotopic chains of Fr [15] and Rn [16] reported fast increase of β with excitation energy. An excitation energy dependent dissipation was also found to be necessary for ^{208}Rn in a Langevin dynamical calculation to fit the prescission neutron multiplicity data [17]. The magnitudes of the dissipation coefficient obtained in the above earlier works [15–17] were much smaller than that obtained in the present work. On the other hand,

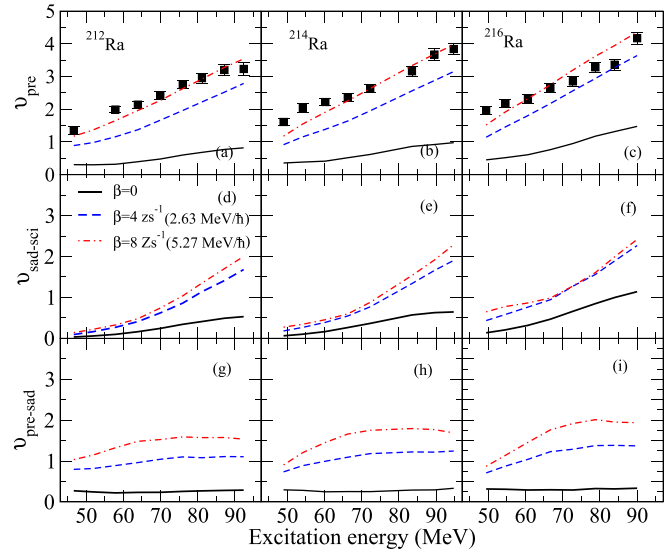

FIG. 6. Calculated ν_{pre} excitation functions for the $^{30}\text{Si} + ^{182,184,186}\text{W}$ reactions for different dissipation strengths are shown in panels (a), (b), (c). Solid squares represent the experimental ν_{pre} for these systems. Similar calculated values of $\nu_{\text{sad-sci}}$ and $\nu_{\text{pre-sad}}$ for different β values are shown in panels (d), (e), (f) and panels (g), (h), (i), respectively.

a strong energy independent dissipation coefficient [10 zs^{-1} (6.58 MeV/$\hbar$)] could reproduce the prescission neutron excitation function for the system $^{30}\text{Si} + ^{197}\text{Au}$ [20]. We briefly discuss here the difference between different analyses yielding different values of β.

While discussing the various effects on neutron multiplicity, we note that the neutron emission probability P_n is given by $P_n = \Gamma_n/(\Gamma_n + \Gamma_f) = (\Gamma_n/\Gamma_f)/[(\Gamma_n/\Gamma_f) + 1]$, where Γ_n and Γ_f are the neutron and fission widths respectively. The charged particle and photon emission widths are much smaller than Γ_n and hence are not included here for the sake of simplification, though they are included in the SM calculations. P_n increases when Γ_n/Γ_f increases.

One important feature which distinguishes the present statistical model analysis (and also that in Ref. [20]) from those performed in Refs. [15,16] is the inclusion of CELD and K degree of freedom in the present work. CELD influences the fission width more strongly than K degree of freedom and, for simplicity, we discuss here the effect of CELD only. CELD increases the Bohr-Wheeler fission width substantially since the collective enhancement is much stronger for the level density ρ_s [Eq. (4)] due to large deformation at saddle compared to the enhancement of ρ_g at the ground state. On the other hand, the effect of CELD on neutron width is moderate since both the parent and daughter nuclei are nearly spherical. Inclusion of CELD thus results in a strong reduction of Γ_n/Γ_f, as illustrated in Fig. 7.

Since the statistical model underestimates the prescission neutron multiplicity when the Bohr-Wheeler fission width, with or without CELD, is used, a damping of the fission width becomes necessary in order to increase Γ_n/Γ_f to fit the experimental data. It is evident from Fig. 7 that a much stronger damping of the Bohr-Wheeler width is necessary when CELD

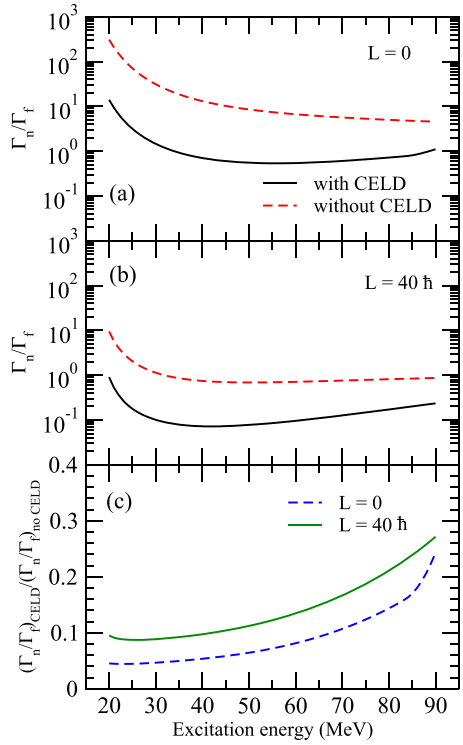

FIG. 7. Ratio of neutron to Bohr-Wheeler fission width for ^{214}Ra obtained with and without CELD in the level densities. Width ratios for compound nuclear spin (L) of 0 and 40$\hbar$ are shown in panels (a) and (b), respectively while panel (c) shows the ratio of the width ratios obtained with and without CELD.

is included in the calculation compared to the case in which CELD is not considered. Therefore, larger values of β are necessary in the present work and in Ref. [20] where CELD is included in the SM calculations compared to the relatively smaller values of β obtained in Refs. [15,16] where CELD was not considered. Similarly, no enhancement of phase space due to collective (rotational and vibrational) was considered in the Langevin dynamical calculation of Ref. [17], and a small dissipation strength was obtained.

To investigate the excitation energy dependence of β obtained with and without CELD in the statistical model calculation, we first observe that CELD introduces an excitation energy dependence in Γ_n/Γ_f as illustrated in the bottom panel of Fig. 7. Inclusion of CELD suppresses Γ_n/Γ_f more strongly at lower excitation energies than at higher ones. Consequently, the degree of enhancement of β obtained with CELD (compared to β obtained without CELD) reduces with increasing excitation energy. Therefore, introduction of CELD neutralizes the increasing trend of β with excitation energy obtained without CELD [15,16] and results in a nearly energy independent β, as observed in the present work.

It is evident from the above discussions that the extracted dissipation strength from analysis of experimental data depends on the choice of different parameters in statistical model calculations. In particular, the excitation energy dependence of calculated decay widths due to inclusion of CELD depends on the choice of various parameters in Eqs. (7) to (9). It

TABLE II. The shell correction energy, the LDM fission barrier, the neutron binding energym and the quadrupole deformation parameter of various Ra isotopes considered in this study are tabulated.

Nucleus	δ_g^p (MeV)	$B_f^{\rm LDM}$ (MeV)	B_n (MeV)	β_2
^{212}Ra	−5.44	6.454	9.10	−0.053
^{214}Ra	−6.34	6.708	8.32	0.0
^{216}Ra	−4.59	6.944	7.31	0.0

further demonstrates the model dependence of the extracted dissipation strength from analysis of experimental data. The statistical model used here being more inclusive, we trust the present work provides a better estimate of nuclear dissipation.

The multiplicities $\nu_{\rm pre\text{-}sad}$ and $\nu_{\rm sad\text{-}sci}$ given in Fig. 6 originate from two distinct processes. While $\nu_{\rm pre\text{-}sad}$ is determined by the competition between fission and evaporation, $\nu_{\rm sad\text{-}sci}$ is the outcome of competition among various evaporation channels during the saddle-to-scission transition time. We first briefly discuss the characteristic features of the multiplicity of presaddle neutrons.

It is observed that $\nu_{\rm pre\text{-}sad}$ increases with β for all three compound nuclei. This is a direct consequence of fission hindrance introduced through the Kramers formula in Eq. (3). A weak dependence of presaddle multiplicity with excitation energy is also noticed. This observation essentially reflects the fact that, with increasing beam energy, larger CN spin states are populated. As the CN spin increases, the fission barrier decreases and the saddle moves towards a more compact configuration, thereby increasing the path from the saddle to the scission. This results in decreasing contributions to $\nu_{\rm pre\text{-}sad}$ and increasing contributions to $\nu_{\rm sad\text{-}sci}$ as CN spin increases. Consequently, the excitation energy dependence of $\nu_{\rm pre\text{-}sad}$ is slow while it is faster for $\nu_{\rm sad\text{-}sci}$. Further, the increase of neutron multiplicity with increasing N/Z may be attributed to the decreasing neutron binding energy of the compound nuclei, The neutron binding energies of ^{212,214,216}Ra are given in Table II. We note here that, in a different approach, presaddle multiplicities were determined from the experimental angular anisotropies and the standard saddle-point statistical model, and were found to decrease with increasing excitation energy [67].

The multiplicity of saddle-to-scission neutrons increases with β as expected since the saddle-to-scission transition time increases with β [Eq. (14)]. It is interesting to note that, though the saddle-to-scission transition time more than doubles as β increases from 4 to 8 zs^{-1} (2.63 and 5.27 MeV/$\hbar$ respectively), the increase of multiplicity is only marginal. This happens because most of the available excitation energy is carried away by evaporation during the interval corresponding to $\beta = 4$ zs^{-1} (2.63 MeV/$\hbar$) leaving a smaller fraction for evaporation in a longer timescale.

Though the experimental $\nu_{\rm pre}$ or the fitted β values do not show any noticeable shell closure effect, we next explore the shell as well as the CELD effects in the SM predictions of multiplicity of prescission neutrons. Two sets of calculations are made, one excluding shell effects in both the level density parameter and the fission barrier and the other excluding CELD in fission and all the evaporation widths. Calculations are made with $\beta = 8$ zs^{-1} (5.27 MeV/$\hbar$) and the results are

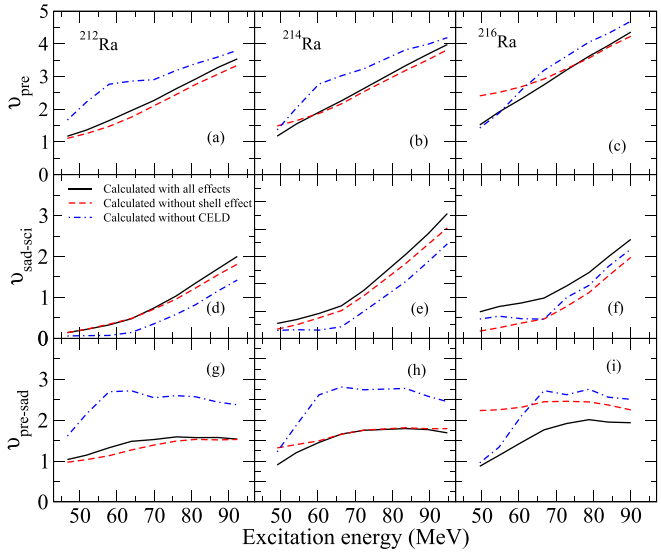

FIG. 8. Effects of shell and CELD in the $\nu_{\rm pre}$ excitation function for the ^{30}Si + ^{182,184,186}W reactions for $\beta = 8$ zs^{-1} (5.27 MeV/$\hbar$) are shown in panels (a), (c), (c). Influence of the aforementioned effects on $\nu_{\rm sad\text{-}sci}$ and $\nu_{\rm pre\text{-}sad}$ for the same dissipation strength are shown in panels (d), (e), (f) and panels (g), (h), (i), respectively.

shown in Fig. 8, where the multiplicities obtained with all the effects are also included.

In order to compare the SM predictions with and without shell effects, we note that Γ_n/Γ_f is approximately determined by the ratio of the leading terms of the respective level densities, and can be written as

$$\frac{\Gamma_n}{\Gamma_f} \approx \frac{e^{2\sqrt{a_g^d(E^i-B_n)}}}{e^{2\sqrt{a_s^p\left(E^i-B_f^{\rm LDM}+\delta_g^p\right)}}} \tag{16}$$

The level density parameter in the ground state of the daughter nucleus is denoted by a_g^d in the above expression, and that of the parent nucleus in the saddle configuration is a_s^p while δ_g^p is the shell correction energy in the ground state of the parent nucleus. B_n and $B_f^{\rm LDM}$ are the neutron binding energy and the LDM fission barrier respectively. Remembering that the shell correction in the level density parameter a_s^p at the saddle is negligible, the shell effect in the above ratio is determined by a_g^d and δ_g^p. The shell correction energy, the LDM fission barrier, and the neutron binding energy of various Ra isotopes are given in the Table II.

When shell correction energies are taken into account, both the numerator (due to a_g^d) and the denominator decrease (δ_g^p being a negative quantity) and hence the shell effect is neutralized to some extent. The extent of neutralization, however, depends on the relative magnitudes of the shell correction energies of the parent and the daughter nuclei. For ^{212}Ra, the shell correction energy of ^{212}Ra is larger than that of ^{211}Ra, being -5.44 and -4.74 MeV respectively. The shell effects are largely neutralized in this case, as we see in Fig. 8(g). Similarly, in the case of ^{214}Ra the shell correction energy of the parent is marginally higher than that of the daughter, which results in a small net effect on $\nu_{\rm pre\text{-}sad}$ [Fig. 8(h)]. For ^{216}Ra, however, this is reversed, since the parent shell correction energy (-4.59 MeV) is smaller than that of the daughter (-5.53 MeV). It gives rise to an appreciable reduction of $\nu_{\rm pre\text{-}sad}$ when shell corrections are included [Fig. 8(i)]. It may further be noted that the reduction is larger at smaller excitation energies, which arises due to the stronger damping of a_g^d at lower excitation energies when the shell correction is included.

In the saddle-to-scission sector, the CN shapes are highly deformed and hence no shell effects are included in the various evaporation widths used to calculate $\nu_{\rm sad\text{-}sci}$. The shell dependence observed in $\nu_{\rm sad\text{-}sci}$ is a consequence of the fact that the excitation energy available in the saddle-to-scission sector depends on $\nu_{\rm pre\text{-}sad}$, which has a shell dependence.

A marginal increase of $\nu_{\rm sad\text{-}sci}$ is observed in calculations including shell effects for ^{212,214}Ra, as shown in Figs. 8(d) and 8(e). It is caused by the lower multiplicity of charged particles in the presaddle stage observed in calculations with shell effects included and which consequently makes higher excitation energy available in the saddle-to-scission sector. For ^{216}Ra, $\nu_{\rm pre\text{-}sad}$ is considerably reduced when shell effects are included, giving rise to larger excitation energies available in the saddle-to-scission sector enabling higher number of neutrons to evaporate.

The effect of excluding CELD is shown in the bottom panels of Fig. 8 where we find that $\nu_{\rm pre\text{-}sad}$ increases substantially for all the three CN. Since CELD is much stronger for highly deformed nuclear shapes such as at the saddle compared to spherical or near-spherical shapes, fission widths increase substantially when CELD is included. Conversely, fission widths reduce when CELD is withdrawn and consequently fission time scale increases allowing emission of more neutrons. The larger number of evaporated neutrons in the pre-saddle stage when CELD is excluded also carries away a larger fraction of excitation energy and thereby making less excitation energy available during the saddle-to-scission transition. Thus, exclusion of CELD causes decrease of $\nu_{\rm sad\text{-}sci}$ as shown in the middle row of Fig. 8. It may be pointed out that we have not considered the effect of CELD on evaporation widths in the above discussion, though they are included in the calculations, because the effects are marginal for the compound nuclei considered here. The nuclei considered here are spherical or nearly spherical as the quadrupole deformations at the ground state of ^{121,214,216}Ra are -0.053, 0.0, and 0.0 respectively [68]. Therefore, the effect of CELD on evaporation process is not significant as has also been observed from studies of evaporation spectra of a spherical nucleus [69].

The CELD and shell effects on the total multiplicity $\nu_{\rm pre}$ are shown in the top row of Fig. 8. As discussed above, both effects primarily impact $\nu_{\rm pre\text{-}sad}$, which modulates the excitation energy and multiplicity in the saddle-to-scission sector in a complementary manner. Thus, the net effects in $\nu_{\rm pre}$ are somewhat reduced compared to those in $\nu_{\rm pre\text{-}sad}$.

VI. SUMMARY AND CONCLUSION

In summary, neutron multiplicity excitation functions from the fission of ^{212,214,216}Ra nuclei are measured to investigate structural and dynamical effects in fission over a wide range of excitation energy. Measured $\nu_{\rm pre}$ values are found to increase

marginally with an increase in N/Z values of the fissioning systems at similar excitation energies. The increase of neutron multiplicity with increasing N/Z may be attributed to the fissility of the CN and the neutron binding energy.

The experimental neutron multiplicities are analyzed within the framework of a statistical model incorporating dynamical hindrance in nuclear fission due to dissipation, shell corrections in the fission barrier and level density, and collective enhancement of level density (CELD). This work shows that the emission of excess neutrons in comparison to the predictions using the Bohr-Wheeler fission width could be accommodated in terms of a strong nuclear dissipation. The dissipation strength required to reproduce the present experimental ν_{pre} data does not show any temperature dependence, unlike that reported in the literature for a few neighboring systems. No isotopic dependence is also observed in the deduced dissipation strength in the present work. A β value of 8 zs^{-1} (5.27 $\text{MeV}/\hbar$) reasonably reproduces the experimental ν_{pre} excitation functions for all three nuclei in the measured excitation energies in this study.

Apart from the effect of dissipation, inclusion of collective enhancement of level density and shell corrections in fission barrier and level density parameters are also found to impact the calculated neutron multiplicities. Though these effects influence the presaddle multiplicities directly, the saddle-to-scission multiplicities are also indirectly affected as a consequence of the changes in the presaddle sector. The net effects on the total pre-scission multiplicities are smaller than those found for the presaddle multiplicities.

The shell effects in the presaddle multiplicity are found to be much larger for ^{216}Ra than for ^{212,214}Ra. The observed shell effects in $\nu_{\text{pre-sad}}$ are qualitatively discussed in terms of the relative magnitudes of the shell correction energies of a CN and the daughter nucleus reached after one neutron emission. The effect of CELD in $\nu_{\text{pre-sad}}$ is large for all three compound nuclei as a result of the large enhancement of level density at the saddle due to its large deformation and consequent enhancement of fission width. Finally we point out that, because fission is essentially a presaddle phenomenon, fission/ER cross sections are also sensitive to the shell and CELD effects. Combined analysis of neutron multiplicities and fission/ER cross sections can therefore reveal more details of various effects in fusion-fission reactions.

ACKNOWLEDGMENTS

The authors gratefully acknowledge the Pelletron and LINAC crew of IUAC, New Delhi for providing excellent quality beam throughout the experiment. Two of the authors (M.S. and A.C.V.) acknowledge Kerala State Council for Science Technology and Environment (KSCSTE) for financial aid in the form of a fellowship. One of the authors (EP) acknowledges DST, Govt. of India for providing support in the form of DST-RFBR Project No. INT/RUS/RFRB/P-266. We acknowledge the DST, Government of India for NAND project under Grant No. IR/S2/PF-02/2007.

[1] L. A. Turner, Rev. Mod. Phys. **12**, 1 (1940).
[2] K.-H. Schmidt and B. Jurado, Rep. Prog. Phys. **81**, 106301 (2018).
[3] M. Thoennessen and G. F. Bertsch, Phys. Rev. Lett. **71**, 4303 (1993).
[4] D. Hilscher and H. Rossner, Ann. Phys. (Paris) **17**, 471 (1992).
[5] A. Gavron, J. R. Beene, B. Cheynis, R. L. Ferguson, F. E. Obenshain, F. Plasil, G. R. Young, G. A. Petitt, M. Jääskeläinen, D. G. Sarantites, and C. F. Maguire, Phys. Rev. Lett. **47**, 1255 (1981).
[6] P. Grange, S. Hassani, H. A. Weidenmuller, A. Gavron, J. R. Nix, and A. J. Sierk, Phys. Rev. C **34**, 209 (1986).
[7] J. Blocki, Y. Boneh, J. R. Nix, J. Randrup, M. Robel, A. J. Sierk, and W. J. Swiatecki, Ann. Phys. (NY) **113**, 330 (1978).
[8] Y. Abe, S. Ayik, P.-G. Reinhard, and E. Suraud, Phys. Rep. **275**, 49 (1996).
[9] P. Fröbrich and I. I. Gontchar, Phys. Rep. **292**, 131 (1998).
[10] K. Mazurek, P. N. Nadtochy, E. G. Ryabov, and G. D. Adeev, Eur. Phys. J. A **53**, 79 (2017).
[11] H. A. Kramers, Physica **7**, 284 (1940).
[12] J. O. Newton, D. J. Hinde, R. J. Charity, J. R. Leigh, J. J. M. Bokhorst, A. Chatterjee, G. S. Foote, and S. Ogaza, Nucl. Phys. A **483**, 126 (1988).
[13] B. B. Back, D. J. Blumenthal, C. N. Davids, D. J. Henderson, R. Hermann, D. J. Hofman, C. L. Jiang, H. T. Penttilä, and A. H. Wuosmaa, Phys. Rev. C **60**, 044602 (1999).
[14] I. Dioszegi, N. P. Shaw, I. Mazumdar, A. Hatzikoutelis, and P. Paul, Phys. Rev. C **61**, 024613 (2000).
[15] V. Singh, B. R. Behera, M. Kaur, A. Kumar, P. Sugathan, K. S. Golda, A. Jhingan, M. B. Chatterjee, R. K. Bhowmik, D. Siwal, S. Goyal, J. Sadhukhan, S. Pal, A. Saxena, S. Santra, and S. Kailas, Phys. Rev. C **87**, 064601 (2013).
[16] R. Sandal, B. R. Behera, V. Singh, M. Kaur, A. Kumar, G. Singh, K. P. Singh, P. Sugathan, A. Jhingan, K. S. Golda, M. B. Chatterjee, R. K. Bhowmik, S. Kalkal, D. Siwal, S. Goyal, S. Mandal, E. Prasad, K. Mahata, A. Saxena, J. Sadhukhan, and S. Pal, Phys. Rev. C **87**, 014604 (2013).
[17] N. Kumar, S. Verma, S. Mohsina, J. Sadhukhan, K. R. Devi, A. Banerjee, N. Saneesh, M. Kumar, R. Mahajan, M. Thakur, G. Kaur, A. Rani, Neelam, A. Yadav, Kavita, R. Kumar, Unnati, S. Mandal, S. Kumar, B. R. Behera, K. S. Golda, A. Jhingan, and P. Sugathan, Phys. Lett. B **814**, 136062 (2021).
[18] J. P. Lestone and S. G. McCalla, Phys. Rev. C **79**, 044611 (2009).
[19] H. Eslamizadeh and H. Falinejad, Phys. Rev. C **105**, 044604 (2022).
[20] M. Shareef, E. Prasad, A. Jhingan, N. Saneesh, K. S. Golda, A. M. Vinodkumar, M. Kumar, A. Shamlath, P. V. Laveen, A. C. Visakh, M. M. Hosamani, S. K. Duggi, P. S. Devi, G. N. Jyothi, A. Tejaswi, P. N. Patil, J. Sadhukhan, P. Sugathan, A. Chatterjee, and S. Pal, Phys. Rev. C **99**, 024618 (2019).
[21] M. D. Usang, F. A. Ivanyuk, C. Ishizuka, and S. Chiba, Phys. Rev. C **94**, 044602 (2016).

[22] M. D. Usang, F. A. Ivanyuk, C. Ishizuka, and S. Chiba, Phys. Rev. C **96**, 064617 (2017).

[23] C. Ishizuka, M. D. Usang, F. A. Ivanyuk, J. A. Maruhn, K. Nishio, and S. Chiba, Phys. Rev. C **96**, 064616 (2017).

[24] L. Meitner, Nature (London) **165**, 561 (1950).

[25] R. Vandenbosch and J. R. Huizenga, *Nuclear Fission* (Academic Press, New York, 1973).

[26] A. N. Andreyev, K. Nishio, and K.-H. Schmidt, Rep. Prog. Phys. **81**, 016301 (2018).

[27] E. Prasad, D. J. Hinde, K. Ramachandran, E. Williams, M. Dasgupta, I. P. Carter, K. J. Cook, D. Y. Jeung, D. H. Luong, S. McNeil, C. S. Palshetkar, D. C. Rafferty, C. Simenel, A. Wakhle, J. Khuyagbaatar, Ch. E. Dullmann, B. Lommel, and B. Kindler, Phys. Rev. C **91**, 064605 (2015).

[28] A. N. Andreyev, J. Elseviers, M. Huyse, P. Van Duppen, S. Antalic, A. Barzakh, N. Bree, T. E. Cocolios, V. F. Comas, J. Diriken *et al.*, Phys. Rev. Lett. **105**, 252502 (2010).

[29] P. Sugathan, A. Jhingan, K. S. Golda, T. Varughese, S. Venkataraman, N. Saneesh, V. V. Satyanarayana, S. K. Suman, J. Antony, R. Shanti, K. Singh, S. K. Saini, A. Gupta, A. Kothari, P. Barua, R. Kumar, J. Zacharias, R. P. Singh, B. R. Behera, S. K. Mandal *et al.*, Pramana **83**, 807 (2014).

[30] S. Venkataramanan, A. Gupta, K. S. Golda, H. Singh, R. Kumar, R. P. Singh, and R. K. Bhowmik, Nucl. Instrum. Methods Phys. Res. Sect A **596**, 248 (2008).

[31] V. E. Viola, K. Kwiatkowski, and M. Walker, Phys. Rev. C **31**, 1550 (1985).

[32] B. E. Watt, Phys. Rev. **87**, 1037 (1952).

[33] D. Hilscher, J. R. Birkelund, A. D. Hoover, W. U. Schröder, W. W. Wilcke, J. R. Huizenga, A. C. Mignerey, K. L. Wolf, H. F. Breuer, and V. E. Viola, Phys. Rev. C **20**, 576 (1979).

[34] V. A. Rubchenya, A. V. Kuznetsov, W. H. Trzaska, D. N. Vakhtin, A. A. Alexandrov, I. D. Alkhazov, J. Äystö, S. V. Khlebnikov, V. G. Lyapin, O. I. Osetrov, Yu. E. Penionzhkevich, Yu. V. Pyatkov, and G. P. Tiourin, Phys. Rev. C **58**, 1587 (1998).

[35] E. Holub, D. Hilscher, G. Ingold, U. Jahnke, H. Orf, and H. Rossner, Phys. Rev. C **28**, 252 (1983).

[36] G. K. S, A. Saxena, V. K. Mittal, K. Mahata, P. Sugathan, A. Jhingan, V. Singh, R. Sandal, S. Goyal, J. Gehlot, A. Dhal, B. R. Behera, R. K. Bhowmik, and S. Kailas, Nucl. Phys. A **913**, 157 (2013).

[37] Y. Aritomo, M. Ohta, T. Materna, F. Hanappe, O. Dorvaux, and L. Stuttge, Nucl. Phys. A **759**, 309 (2005).

[38] M. Thakur, B. R. Behera, R. Mahajan, G. Kaur, P. Sharma, K. Kapoor, K. Rani, P. Sugathan, A. Jhingan, N. Saneesh, R. Dubey, A. Yadav, A. Chatterjee, M. B. Chatterjee, N. Kumar, S. Mandal, S. K. Duggi, A. Saxena, S. Kailas, and S. Pal, Phys. Rev. C **98**, 014606 (2018).

[39] A. C. Berriman, D. J. Hinde, M. Dasgupta, C. R. Morton, R. D. Butt, and J. O. Newton, Nature (London) **413**, 144 (2001).

[40] R. du Rietz, E. Williams, D. J. Hinde, M. Dasgupta, M. Evers, C. J. Lin, D. H. Luong, C. Simenel, and A. Wakhle, Phys. Rev. C **88**, 054618 (2013).

[41] E. Prasad, D. J. Hinde, E. Williams, M. Dasgupta, I. P. Carter, K. J. Cook, D. Y. Jeung, D. H. Luong, C. S. Palshetkar, D. C. Rafferty, K. Ramachandran, C. Simenel, and A. Wakhle, Phys. Rev. C **96**, 034608 (2017).

[42] P. K. Sahu, R. G. Thomas, A. Saxena, R. K. Choudhury, S. S. Kapoor, L. M. Pant, M. Barbui, M. Cinausero, G. Prete, V. Rizzi, D. Shetty, D. Fabris, M. Lunardon, S. Moretto, G. Viesti, G. Nebbia, S. Pesente, B. Dalena, G. D'Erasmo, D. Di Santo, E. M. Fiore, M. Palomba *et al.*, Phys. Rev. C **72**, 034604 (2005).

[43] R. G. Thomas, A. Saxena, P. K. Sahu, R. K. Choudhury, I. M. Govil, S. Kailas, S. S. Kapoor, M. Barbui, M. Cinausero, G. Prete, V. Rizzi, D. Fabris, M. Lunardon, S. Moretto, G. Viesti, G. Nebbia, S. Pesente, B. Dalena, G. D'Erasmo, E. M. Fiore, M. Palomba *et al.*, Phys. Rev. C **75**, 024604 (2007).

[44] T. Banerjee, S. Nath, and S. Pal, Phys. Lett. B **776**, 163 (2018).

[45] V. Weisskopf, Phys. Rev. **52**, 295 (1937).

[46] M. Blann, Phys. Rev. C **21**, 1770 (1980).

[47] J. P. Lestone, Phys. Rev. C **59**, 1540 (1999).

[48] J. Sadhukhan and S. Pal, Phys. Rev. C **78**, 011603(R) (2008).

[49] N. Bohr and J. A. Wheeler, Phys. Rev. **56**, 426 (1939).

[50] K. Hagino, N. Rowley, and A. T. Kruppa, Comput. Phys. Commun. **123**, 143 (1999).

[51] Ó. Akyüz and A. Winther, in *Nuclear Structure and Heavy-Ion Collisions*, *Proceedings of the International School of Physics "Enrico Fermi", Course LXXVII, Varenna, Italy, 1979*, edited by R. A. Broglia, C. H. Dasso, and R. Richi (North-Holland, Amsterdam, 1981).

[52] D. J. Hinde, A. C. Berriman, R. D. Butt, M. Dasgupta, I. I. Gontchar, C. R. Morton, A. Mukherjee, and J. O. Newton, J. Nucl. Radiochim. Sci. **3**, 31 (2002).

[53] A. J. Sierk, Phys. Rev. C **33**, 2039 (1986).

[54] K. Mahata, S. Kailas, and S. S. Kapoor, Phys. Rev. C **92**, 034602 (2015).

[55] W. D. Myers and W. J. Swiatecki, Nucl. Phys. **81**, 1 (1966).

[56] P. Möller, A. J. Sierk, T. Ichikawa, and H. Sagawa, At. Data Nucl. Data Tables **109-110**, 1 (2016).

[57] W. Reisdorf, Z. Phys. A **300**, 227 (1981).

[58] S. Bjørnholm, A. Bohr, and B. R. Mottelson, *Proceedings of the International Conference on the Physics and Chemistry of Fission, Rochester, 1973* (IAEA, Vienna, 1974), Vol. 1, p. 367.

[59] T. Banerjee, S. Nath, and S. Pal, Phys. Rev. C **99**, 024610 (2019).

[60] A. V. Ignatyuk, G. N. Smirenkin, M. G. Itkis, S. I. Mulgin, and V. N. Okolovich, Sov. J. Part. Nucl. **16**, 307 (1985).

[61] V. I. Zagrebaev, Y. Aritomo, M. G. Itkis, Yu. T. Oganessian, and M. Ohta, Phys. Rev. C **65**, 014607 (2001).

[62] M. Ohta, in *Proceedings on Fusion Dynamics at the Extremes, Dubna, 2000*, edited by Yu. T. Oganessian and V. I. Zagrebaev (World Scientific, Singapore, 2001), p. 110.

[63] A. R. Junghans, M. de Jong, H.-G. Clerc, A. V. Ignatyuk, G. A. Kudyaev, and K.-H. Schmidt, Nucl. Phys. A **629**, 635 (1998).

[64] P. Grangé, L. Jun-Qing, and H. A. Weidenmüller, Phys. Rev. C **27**, 2063 (1983).

[65] K. H. Bhatt, P. Grangé, and B. Hiller, Phys. Rev. C **33**, 954 (1986).

[66] H. Hofmann and J. R. Nix, Phys. Lett. B **122**, 117 (1983).

[67] S. Soheyli and M. K. Khalili, Phys. Rev. C **87**, 034610 (2013).

[68] P. Möller, A. J. Sierk, T. Ichikawa, and H. Sagawa, At. Data Nucl. Data Tables **109**, 204 (2016).

[69] D. Pandit, B. Dey, S. Bhattacharyal, T. K. Rana, D. Mondal, S. Mukhopadhyay, S. Pal, A. De, P. Roy, K. Banerjee, S. Kundu, A. K. Sikdar, C. Bhattacharya, and S. R. Banerjee, Phys. Lett. B **816**, 136173 (2021).